Molecular dynamics (MD) investigations of preformed structures of the transmembrane domain of the oncogenic Neu receptor dimer in a DMPC bilayer

ARTICLE *in* BIOPOLYMERS · APRIL 2005

Impact Factor: 2.39 · DOI: 10.1002/bip.20176 · Source: PubMed

4 AUTHORS, INCLUDING:

Pierre Aller
Diamond Light Source
22 PUBLICATIONS **220** CITATIONS
SEE PROFILE

Norbert Garnier
Université d'Orléans
29 PUBLICATIONS **219** CITATIONS
SEE PROFILE

Pierre Aller[1]
Loïs Voiry[1]
Norbert Garnier[2]
Monique Genest[1]
[1] *Centre de Biophysique Moléculaire, UPR 4301, CNRS, rue Charles Sadron, 45071 Orléans Cedex 02, France*

[2] *University of Orléans, Orléans, France*

Molecular Dynamics (MD) Investigations of Preformed Structures of the Transmembrane Domain of the Oncogenic Neu Receptor Dimer in a DMPC Bilayer

Received 31 August 2004; accepted 7 October 2004
Published online 19 January 2005 in Wiley InterScience (www.interscience.wiley.com). DOI 10.1002/bip.20176

Abstract: *The critical Val/Glu mutation in the membrane spanning domain of the rat Neu receptor confers the ability for ligand-independent signaling and leads to increased dimerization and transforming ability. There is evidence that the two transmembrane interacting helices play a role in receptor activation by imposing orientation constraints to the intracellular tyrosine kinase domains. By using MD simulations we have attempted to discriminate between correct and improper helix–helix packing by examining the structural and energetic properties of preformed left-handed and right-handed structures in a fully hydrated DMPC bilayer. The best energetic balance between the residues at the helix–helix interface and the residues exposed to the lipids is obtained for helices in symmetrical left-handed interactions packed together via Glu side chain/Ala backbone interhelical hydrogen bonds. Analyses demonstrate the importance of the ATVEG motif in helix–helix packing and point to additional contacting residues necessary for association. Our findings, all consistent with experimental data, suggest that a symmetrical left-handed structure of the helices could be the transmembrane domain configuration that promotes receptor activation and transformation. The present study may provide further insight into signal transduction mechanisms of the ErbB/Neu receptors.* © 2005 Wiley Periodicals, Inc. Biopolymers 77: 184–197, 2005

Keywords: *tyrosine kinase receptor; transmembrane helix; helix–helix packing; MD simulations; membrane environment; α–π motif*

INTRODUCTION

ErbB receptors play a prominent role in the control of a variety of cellular processes during embryonic development and in the regulation of many metabolic and physiological processes.[1,2] Normal signaling of these receptors (ErbB1/HER1, the epidermal growth factor receptor EGFR, ErbB2/HER2/Neu, ErbB3/HER3, and ErbB4/HER4) involves ligand-induced dimerization and tyrosine autophosphorylation in the catalytic domain for enhanced kinase activity.[3] The receptor dimerizes either with a like member of the family or with another member leading to homo- or heterodimers allowing diversity in signaling. All the

Correspondence to: M. Genest; email: m.genest@cnrs-orleans.fr

ErbB members are involved in human cancer. ErbB2 has no known ligand and serves a coreceptor or a preferred heterodimerization partner for other members, explaining its aberrant signaling. ErbB2 is the cause of approximately 30% of invasive cancers.[4]

ErbB receptors are single-chain modular glycoproteins and have in common an extracellular ligand-binding region, a single transmembrane domain, and an intracellular tyrosine kinase domain flanked by a juxtamembrane region and a C-terminal regulatory tail. X-ray structures of extracellular portions of EGFR, HER2/Neu, HER3[5–11] and of the EGFR kinase domain[12] help in the understanding of receptor signaling. However, the molecular mechanisms by which the transmembrane domain mediates receptor activity remain unknown.

The Neu protooncogene, the rodent ortholog of ErbB2, is an example of bitopic membrane protein of this family that oligomerizes due to its transmembrane domain. The single Val to Glu substitution in the membrane spanning sequence renders the receptor constitutively activated.[13–15] It was shown that receptor dimerization is not sufficient for signaling[16,17] and that correct position of the tyrosine kinase domains needs to be adjusted for further signal transduction. Strong support exists of the role of the transmembrane domain as rotational linker[18] and it was suggested that it imposes constraints on the juxtamembrane region constituted by the amino terminal of the kinase domain.[19,20]

The transmembrane domain of ErbB receptors is a site for targeting the binding of agents capable of inhibiting receptor activation[21] and strategies toward inhibition and prevention of receptor activation imply structural studies.[22] The structure of the transmembrane domain in the active receptor may provide insights into the reorientation mechanisms and opportunities for the design of novel anticancer agents.

Solid state NMR methods and Fourier transformed infrared (FTIR) spectroscopy were applied to the oncogenic Neu transmembrane domain reconstituted into POPC (palmitoleoyl-phosphatidylcholine) : POPS (palmitoleoylphosphatidylserine) membranes.[23] Measurements of short interhelical distances involving Glu and Gly residues provided structural constraints for defining a right-handed model of the two helices in the active dimer. A similar structure was proposed for the wild-type Neu transmembrane dimer. However, Monte Carlo energy minimization techniques have contradicted this conclusion[24] by suggesting a left-handed structure for the wild-type dimer compatible with the Glu mutation and in total agreement with interfacial residues identified from experiments.[16,23,25] These two models differ by the packing of the two helices, one with a right-handed GpA-like packing, the other with the two helices wrapped around one another in a left-handed supercoil.

The same controversy exists regarding the ErbB2 transmembrane domain. While Monte Carlo techniques demonstrate a left-handed structure with helices crossed at the N-terminus utilizing a GxxxG-like motif,[24] conformational search based on the presence of Gly and small residues at helix–helix interface favors a right-handed structure.[26] GxxxG motif mediates right-handed interactions,[27,28] the best model being the glycophorin A dimer[29,30] but may completely abolish dimerization[31] or mediate left-handed helix–helix association.[32,33]

In addition, molecular dynamic (MD) simulations on the oncogenic ErbB2/Neu transmembrane domain dimers[34–36] revealed a left-handed structure similar to that predicted from Monte Carlo studies.[24]

Both these results contribute to considerable confusion on how the two ErbB2/Neu transmembrane helices self-associate. Helix–helix packing is a key for inducing the correct orientation of the catalytic domains for dimer activation. Helices crossed in a right-handed or a left-handed fashion necessarily impose different directions to the C-termini of the transmembrane dimer and consequently to the catalytic domain via the juxtamembrane domain.

Because experimental data are not sufficient to properly define helix–helix packing, we have examined the behavior of preformed structures of the oncogenic Neu transmembrane dimer (Neu^{E}_{TM} dimer) in a membrane bilayer composed of hydrated DMPC (dimyristoyl-phosphatidylcholine) molecules using MD simulation techniques. In support of the choice of different structures is the evidence that ErbB family members exist as preformed dimers.[37]

Large-scale changes in helix–helix packing could not be expected during several nanosecond simulations.[38] Nevertheless, we are convinced that essential features can be described on the time scale of the present simulations to gain further insight into dimer properties such as interactions with the lipid environment. Six different dimer models have been studied, four having a left-handed structure and two having a right-handed structure. All these models are derived either from MD calculations consistent with experimental data[35] or from experiments.[16,23]

The overall results shows that a symmetrical structure of the dimer with helices in left-handed interactions is that which provides the best energetic compromise between helix–helix packing and residues exposed to the lipids. Results are discussed in relation with experimental data.

MATERIALS AND METHODS

General Setup

The simulation methodology used in the present work follows the general protocol developed for the insertion of gramicidin channel,[39,40] melittin,[41] and bacteriophage Pf1 coat protein[42] in a lipid bilayer. This same protocol was recently used for the study of the transmembrane domain of the oncogenic ErbB2 receptor dimer in a DMPC bilayer.[36]

The sequence of the transmembrane domain of the oncogenic Neu receptor used in the simulations is the following: E_{650}QRASPVTFIIATVE_{664}GVLLFLILVVVVGILIK-RRR$_{684}$ where the Glu664 mutation replaces the Val residue in the protooncogenic receptor. This 35-residue sequence includes the putative hydrophobic transmembrane region Val656-Ile680 flanked at the N-terminus by 6 residues, 3 of which are strongly polar and at the C-terminus by 4 basic residues serving as signal sequence for membrane anchoring at the cytoplasmic side. The peptide sequence was capped by a methyl acetamide group and a methyl amide group at the N- and the C-terminal ends, respectively.

The juxtamembrane residues Glu, Lys, and Arg were charged while Glu664 at the mutation site was considered to be in a protonated state in agreement with experimental data.[43] To ensure the neutrality of the transmembrane peptide 6 counterions (1 Na^+, 5 Cl^-) were added and initially placed at a distance of 2.5 Å from the heavy atom (C, O, or N) of the charged group at the side chain extremity.

The Neu^E_{TM} dimer/DMPC bilayer microscopic system consists of a preformed homodimer (two transmembrane helices with their 6 counterions each), 64 DMPC (32 in each layer), and about 2,700 water molecules. A total of about 17,000 atoms constitutes the initial cell for the simulation with the dimensions 48, 48, and 72 Å along the *X*-, *Y*-, and *Z*-axes, respectively. This central unit of the system gives a cross-sectional area of 64 $Å^2$ per DMPC molecule[44] and a water/lipid ratio of 40:1.[45] Periodic boundary conditions in three dimensions were used. The membrane normal is oriented along the *Z*-axis and the center of the bilayer is placed at $Z = 0$. Calculations were run with the program CHARMM Version 26[46] and the all hydrogen PARAM 22 force field,[47,48] which includes the phospholipid library[49] and the TIP3P water potential.[50]

The average temperature of the system was set to 330 K, well above the gel–liquid crystal phase transition of DMPC[51] to ensure that the bilayer was in the liquid crystalline state. A similar temperature was used in other simulations of proteins inserted into DMPC bilayers with convincing results.[36,52,53] A high temperature will also increase atomic fluctuations[54] and lead to a better exploration of dynamic events occurring on a short simulation time. For all the simulations the SHAKE algorithm[55] was used to fix all bonds involving hydrogen atoms. The time step of integration was 2 fs.

Six different Neu^E_{TM} dimer/DMPC systems corresponding to six distinct initial dimer models have been simulated for a total duration of 4.8 ns each. The dimer structures are described below.

Each Neu^E_{TM} dimer/DMPC system was first preequilibrated over 140 ps of Langevin dynamics followed by equilibration during 1,250 ps in the microcanonical ensemble with constant energy and volume (NVE ensemble). Nonbonded interactions were truncated at 11 Å and electrostatic interactions switched off over a distance of 3 Å. Velocity rescaling (10 ps) was applied to adjust the temperature at 330 K before continuing the simulation in the NP_nAT ensemble [constant normal pressure (P_n), surface area (A), and temperature (T)] for 3,540 ps. The NP_nAT conditions allow the *Z* dimension of the simulation box to vary by controlling the normal pressure P_n and thus leaving the membrane thickness free to adjust while the *X* and *Y* dimensions are fixed.[36,54,56,57] During this period full electrostatic interactions were calculated using Ewald sums[58] and van der Waals interactions were truncated at 10 Å. The trajectory consisted of data collection (coordinates and energy values) taken every 0.5 ps step.

The control of the geometrical parameters of the dimer along the NP_nAT simulation was performed over different time ranges giving rise to very similar results. We then chose to present the results obtained over the last nanoseconds of the simulation [each simulation covers 4.8 ns including the equilibration period (NVE ensemble and rescaling) and the production period (NP_nAT ensemble)].

All of the Neu^E_{TM} dimer/DMPC simulations and analyses were carried out on a multiprocessor platform (Linux Beowulf clusters composed of 4 nodes each having dual 1 GHz Pentium III processors and composed of 6 nodes each having dual Athlon MP2200+ processors).

Initial Neu^E_{TM} Dimer Structures

Six distinct structures of the Neu^E_{TM} dimer were studied: four are left-handed coiled coils and two are right-handed coiled coils. A schematic representation of these models is given in Figure 1 along with the definition of the handedness of the helices.[59]

The left-handed models were obtained from previous MD simulations performed in vacuo[35] starting either from two parallel ideal helices or wrapped around each other in a left sense similarly to the GCN4 leucine zipper.[60] All models are compatible with interhelical hydrogen bonds involving the Glu residues. One dimer structure is symmetrical and exhibits helices related by a local twofold axis resulting in identical helix faces at the dimer interface. This model, named L_{dd}, is characterized by the position of the Glu residues at the inner interface at position **d** of the heptad repeat (**abcdefg**$_n$). The three other left-handed models, named L_{da}, L_{ga}, and L_{de}, have a nonsymmetrical interface (asymmetrical dimer) with Glu at position **a**, **d**, **e,** or **g** at the interface [L_{da} is a left-handed structure (L) with one Glu residue at position **d** on one helix H1 (or the second helix H2) and the other Glu residue at position **a** on H2 (or H1)].

The two right-handed coiled coils exhibit a symmetrical helix–helix interface. One, referred to as R_A, results from MD simulation[35] starting from initial parallel ideal helices with the two Val656 residues in a symmetrical position at

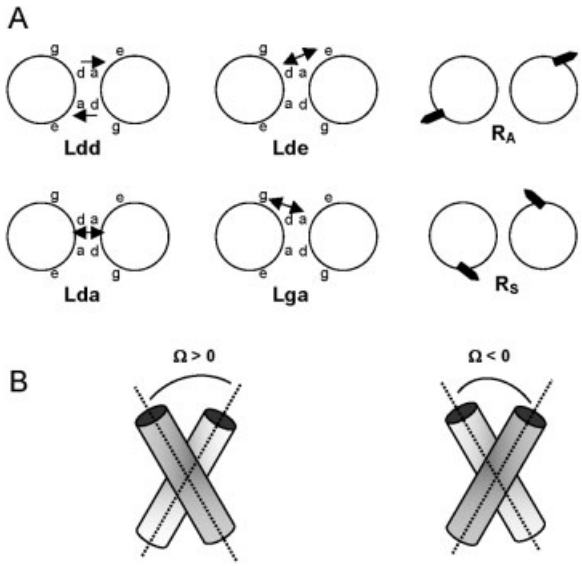

FIGURE 1 (A) Schematic representation of the initial structures of the Neu^E_{TM} dimers used for the simulations in a DMPC environment. Each helix is represented by a cylinder viewed from the N-terminus along the helical axis. L_{dd}, L_{da}, L_{de}, and L_{ga} designate left-handed models derived from in vacuo MD simulations.[35] The Glu residues are at position **a**, **d**, **e**, or **g** of the heptad repeat $(\mathbf{abcdefg})_n$ characteristic of helices crossed in a left-handed sense. The arrows indicate interhelical hydrogen bonds involving the two Glu side chains (↔) or one Glu side chain and the carbonyl group of Ala661(←). R_A (from an in vacuo MD simulation[35]) and R_S (proposed from NMR data[23]) designate right-handed models. The thick line indicates the direction of the Cα–Cβ bond of the Glu side chain. (B) Definition of the left and right handedness of helix–helix dimers according to Chothia et al.[59] If the top helix (dark grey) is rotated counterclockwise with respect to the bottom helix, the crossing angle Ω is positive and characterizes a left-handed structure. If the top helix is rotated clockwise with respect to the bottom helix, the crossing angle Ω is negative and characterizes a right-handed structure. By this definition, the direction of the helices is ignored.

the dimer interface as predicted from cysteine scanning studies.[16] This right-handed model is the only one obtained from a previous computational search whereas all others converge to helices in left-handed interactions.[35]

The second model, R_S, is the Neu^E_{TM} dimer structure derived from NMR studies.[23] For all these initial models each monomer approaches the ideal α-helix structure.

It is reasonable to think that these six dimer structures, with Glu at the inner dimer interface and at the peripheral position of the interface, give a good representation of the possible helix–helix arrangements.

Neu^E_{TM} Dimer /DMPC System

The construction of the initial configuration of a Neu^E_{TM} dimer/DMPC followed the general protocol developed by Woolf and Roux.[39–42] The dimer was inserted perpendicular to the membrane plane (dimer axis parallel to the *Z* direction). The six first residues were embedded into the membrane interface of the upper leaflet (N-terminal side) and the Pro residues were positioned close to the mean plane of the phosphorous atoms. The hydrophobic region of the transmembrane sequence totally traverses the hydrophobic core of the bilayer and the C-terminal Lys and Arg residues are located into the hydrophilic part of the lower leaflet. This position of the two helices in the DMPC bilayer respects the preferred location of transmembrane residues.[61–63]

The lipid head groups were first represented by Lennard-Jones spheres. The position of the center of the spheres at $Z = \pm 17$ Å corresponds to a phosphate–phosphate distance (D_{PP}) equal to 34 Å representative of the DMPC bilayer thickness in fluid phase.[64] Successive minimization steps and short MD simulations were applied to optimize the van der Waals contacts between the spheres. They then were replaced by explicit DMPC molecules in a initial configuration arbitrarily chosen from a preequilibrated and prehydrated lipid library.[65] The lipid positions were optimized in the three directions (rotation along *Z* and translation in the *XY* plane) before completing the construction of the bilayer by water layers (bulk). The resulting DMPC bilayer, which assembles 64 lipids (32 in each layer), water, counterions, and the two Neu^E_{TM} helices, simulates a good packing in the central box. Successive minimizations and MD runs gave an initial configuration of the system that was used as a starting point for MD simulations.

Simulation Conditions

During the thermalization period planar harmonic restraints were applied to the phosphorous atoms of the DMPC to keep them close to the $Z = \pm 17$ Å planes. Harmonic restraints were also applied to the water oxygen atoms to prevent early water penetration into the membrane. To ensure a smooth relaxation of the system, all atoms of the helices were first restrained to their initial position. These restraints were gradually reduced during the Langevin dynamics and finally removed.

During the NVE equilibration planar harmonic restraints were applied to the center of mass of the DMPC molecules in the *Z* direction to prevent any global drift (force constant of 5 kcal/mol/Å^2). To prevent lateral drift of the dimer but allow reasonable helix motions, soft cylindrical restraints (force constant of 5 kcal/mol/Å^2) were applied to the center of mass of one helix (H1 was arbitrarily chosen). This protocol was found to be more efficient than the use of cylindrical restraints applied on the center of mass of each helix or on the center of mass of the dimer, which severely restrict helix motions into the bilayer and conformational changes of helical backbone. However, for the right-handed dimers, R_A and R_S, large helix distortions were observed at the beginning of the simulations. To avoid early helix uncoiling the α-helical hydrogen bond network was maintained through soft distance restraints applied between the

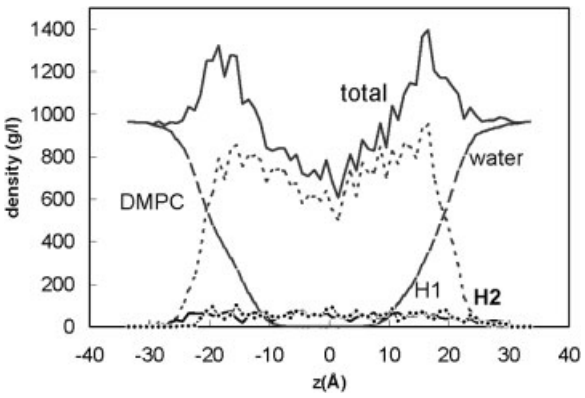

FIGURE 2 Average atomic density profiles of the main components of the DMPC bilayer including the Neu^{E}_{TM} dimer (model L_{dd}). The density profiles of the two helices H1 (●) and H2 (thick line) are shown individually. In the case of L_{dd} the C-terminal end ($Z < 0$) of H2 goes deeper than H1 into the membrane interface. Similar average atomic density profiles are observed for the different Neu^{E}_{TM} dimer/DMPC systems.

carbonyl oxygen atom of residue i and the corresponding nitrogen atom of residue $i + 4$. The force constant values were progressively reduced from 50 to 0 kcal/mol/Å^2 at the end of the NVE period and the simulation was pursued without intrahelical hydrogen bond restraint.

During the NP_nAT simulation, the extended system method described by Hoover[66] and implemented in CHARMM was used. Normal pressure P_n, pressure piston mass, and the Langevin piston collision frequency equal 1 atm, 750 amu, and 5 ps^{-1}, respectively. The thermal piston mass was set to 3,000 kcal.ps^2. The average height of the simulation box was monitored for equilibration criteria. The values vary from 72.8 to 73.8 Å with small fluctuations of 0.3 Å depending on the simulated system. During the whole production trajectory the soft restraints applied to the DMPC molecules and to helix H1 were maintained. No other restraint was applied.

RESULTS

Atomic Density Profiles

As a control of the quality of the bilayer model, we have calculated the atomic density profiles of water, lipids, and peptides for the six different Neu^{E}_{TM}/DMPC systems. The density profile of the pure DMPC bilayer performed in the same simulation conditions was given previously.[36] The averaged properties of the DMPC bilayer including the Neu^{E}_{TM} dimer L_{dd} are shown in Figure 2. The lipid head group peak–peak distance is about 35.0 ± 2.0 Å and the phosphate–phosphate distance (D_{PP}) between the two layers is 35.8 ± 0.4 Å. During the simulation the D_{PP} spacing increases by about 2.0 Å as previously observed from a pure DMPC bilayer simulation and including the $ErbB2^{E}_{TM}$ dimer.[36] These average values are in good agreement with those reported from experiments on fluid DMPC bilayer.[45,67] The distribution of the DMPC density is minimum at the center of the bilayer consistent with experimental measurements.[68] The water density increases in the region of the lipid–water interface and converges toward the normal bulk density. No water molecule traverses the membrane, the deepest penetration being to within 6 Å of the center of the bilayer (at $Z = 0$ Å).

Similar density profiles were obtained for the other Neu^{E}_{TM} dimer/DMPC systems, indicating that the helices are well inserted into the bilayer with the hydrophobic Val656-Ile680 sequence completely embedded into the bilayer core.

Structural Features

Helix–helix crossing and helix tilt. Snapshots of the six different Neu^{E}_{TM} dimer/DMPC systems at the end of the simulation (Figure 3) show that the dimers do not remain perpendicular to the membrane plane and that the left-handed or the right-handed helix arrangement is maintained throughout the simulation.

As observed in Figure 4, helix–helix crossing angles range from 6 to 15° around the average value with a standard deviation of about 3°. Interestingly, for the left-handed models, the helices cross with an angle between 33 and 38° on average, slightly larger than in the initial structure except for L_{dd}. The right-handed models have a crossing angle of −30° on average with a deviation of ~ 10° from the initial structure with an increase of the angle (absolute value) in R_A and a decrease in R_S. Average tilt angles of the left-handed dimers range from 8 to 11° relative to the membrane normal, with fluctuations comparable to those of the crossing angles. The right-handed dimer R_S remains almost parallel to the membrane normal with the smallest tilt angle (around 6°) while dimer R_A is more tilted (around 16°). Except for L_{ga}, the tilt of the dimers is relatively well stabilized after 2.5 ns.

The L_{ga} simulation results in helices with a distance of closest approach smaller than the predicted in vacuo simulation by about 1.4 Å. In all other cases this distance is larger, from 0.5 to 1.2 Å, leading on average a value of ~ 8 Å. These average values are close to those observed in membrane proteins.[69]

The root mean square deviation (RMSD) calculated on the Cα atoms of the Val656-Ile680 sequence from the initial structure is around 2 Å on average throughout the simulation with the exception of dimer

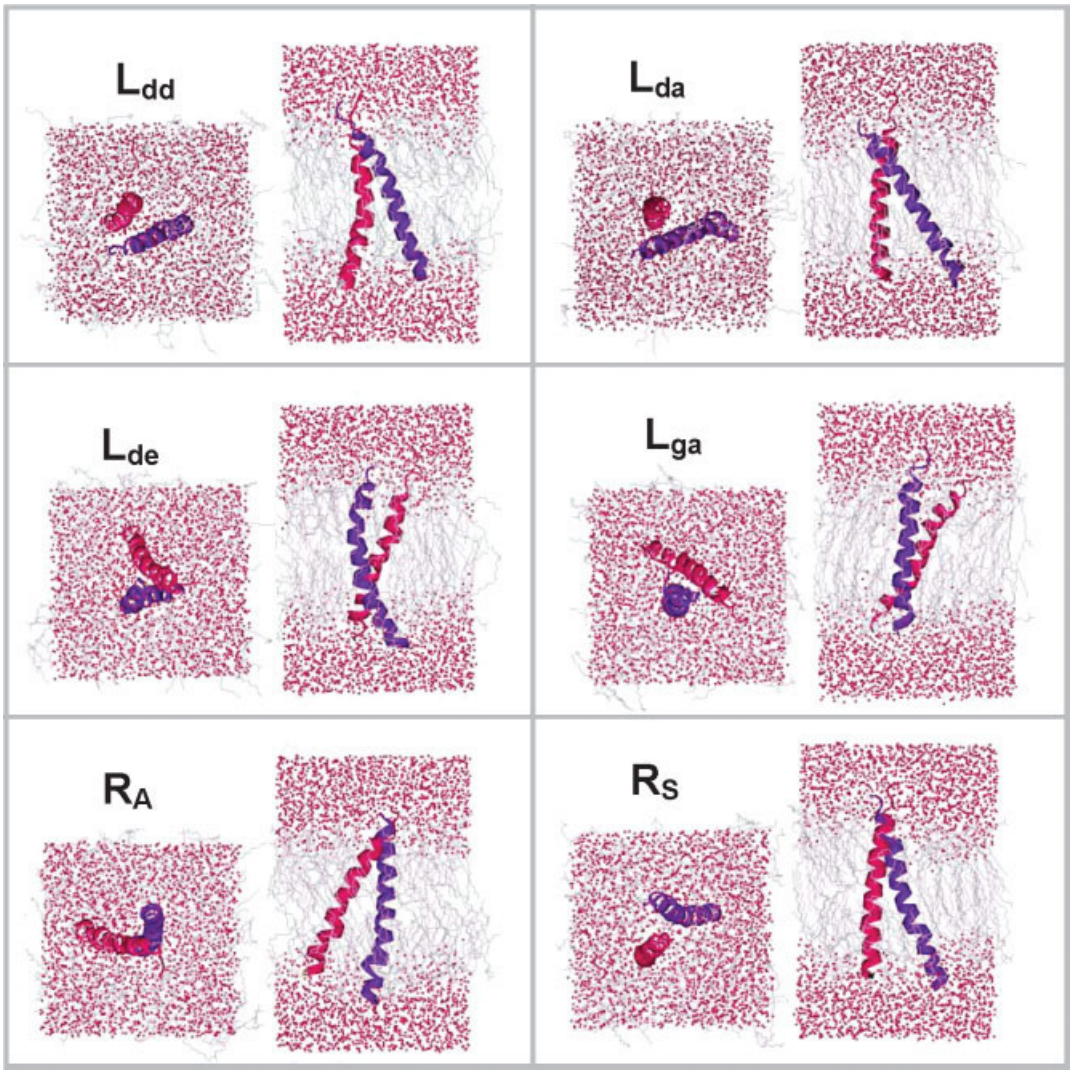

FIGURE 3 Snapshots of the Neu^{E}_{TM} dimers embedded in a DMPC bilayer at the end of a 4.8-ns MD simulation. Helices are in a ribbon representation (blue H1; red H2), the lipids are drawn with thin gray lines, and water is drawn with small red spheres. Each dimer is viewed in the *ZY* plane of the bilayer (*Z*-axis = membrane normal) to evidence the tilt of the helices [N-terminus (top) C-terminus (bottom)] (right picture) and in the XY plane (membrane plane) to illustrate the left-handed interactions in L_{dd}, L_{da}, L_{de}, and L_{ga} and the right-handed interactions in R_A and R_S (left picture). The view is along the *Z*-axis from the N-terminus to the C-terminus.

L_{ga} with a lower value (1.3 Å) and dimer R_A with the highest, around 3 Å.

Helix Structure. During the simulation, each monomer in a dimer retained the α-helical structure except for minor disruptions at helix ends. Unwinding of the helical structure is mainly due to the presence of Pro655 at the N-terminus preventing α-HB formation. At the C-terminal end α-helical deviations are less pronounced and suggest side chain mobility.

Helices undergo π distortions within the hydrophobic sequence embedded in the bilayer core. Figure 5 shows the residence time of the π H-bonds formed during the last nanosecond of the simulation. These π H-bonds are observed at the N-terminus of one monomer in L_{da} and involve Pro655 and Val656 and in L_{de} at the level of Ile659-Ile660. The carbonyl group of Ile660 is hydrogen bonded to the NH group of Gly665, resulting in a π bulge encompassing the Glu mutation. Such π distortion was detected from previous simulations and allows interhelical H-bonds between the two Glu side chains. Interestingly π helical deformations frequently occur at the level of the Val-rich sequence. Such π helical tendencies have been already

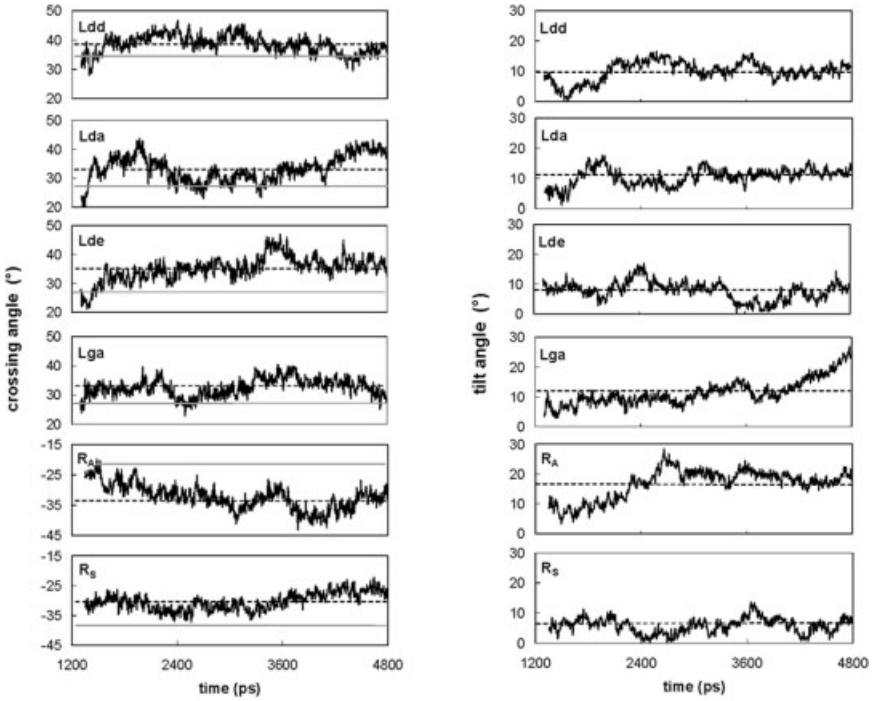

FIGURE 4 (Left) Helix–helix crossing angle (Ω) of the Neu^{E}_{TM} dimer models throughout the NP_nAT simulation (left-handed model: $\Omega > 0$; right-handed model: $\Omega < 0$[59]). The values (°) are calculated on the 35-residue sequence. For the left-handed models (L_{dd}, L_{da}, L_{de}, and L_{ga}), the helices cross with an angle between 33 and 38° on average. The crossing angle is around −30° for the two right-handed models R_A and R_S. Gray line, starting structure; dotted line; simulation average. (Right) Tilt angle (°) relative to the membrane is normal (*Z*-axis). Except for L_{ga} the tilt of the dimers is relatively well stabilized after 2.5 ns.

reported in previous theoretical studies[70] and were recently confirmed from experimental NMR studies.[71,72]

Interhelical H-Bonds. Glu at the dimer interface allows two types of H-bond connections across the dimer: H-bonds are formed between the two Glu side chains or between one side chain and the carbonyl main chain atom of Ala661. Glu side chain to backbone H-bonds are particularly strong in dimer L_{dd} and occur 75 to 85% of the time over the last nanosecond for each monomer, respectively. They occur only 35% of the time for one monomer in dimer R_S. Glu on the second monomer is hydrogen bonded to the Thr662 side chain via water molecules. In dimer L_{da}, side chain–side chain H-bonds are asymmetrical and persist 45 to 90% for each monomer. They are not often observed in L_{de} and L_{ga} (less than 5 to 10%, respectively) owing to the peripheral position of one Glu at the dimer interface.

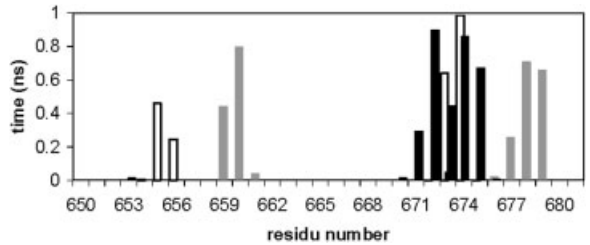

FIGURE 5 Residence time of π H-bonds observed in dimers L_{da} (white), L_{de} (gray), and R_A (black). π H-bonds are often observed at the level of the Val673-Val676 sequence. In R_A they occur in the two helices. The criteria used for H-bond formation are O(CO)–H(NH) distance $\leq$ 2.4 Å and N–H–O angle $\geq$ 130°.

Ser and Thr residues at the N-terminal side exhibit both intramolecular and intermolecular H-bonds. However, these are few (observed less than 6% of the time), except in dimer L_{ga}, where hydroxyl connections between Ser654 and Thr657 exist around 30% of the time.

Juxtamembrane residues are also involved in interhelical H-bonds when the side chains are favorably oriented toward the dimer interface. At the N-terminus both the Glu650 and Arg652 side chains on each monomer are symmetrically hydrogen bonded almost all along the R_S simulation, operating as a key at the

Table I Helix–Helix and Motif (ATVEG)–Helix Interactions[a]

Dimer models	Helix–Helix Interactions			Motif–Helix Interactions			Dimer Stability		
	E_{VdW}	E_{Elec}	E_{Inter}	E_{VdW}	E_{Elec}	E_{Inter}	E_{Intra}	E_{Stress}	E_{Tot}
L_{dd}	−26.5	−8.3	−34.8	−8.4	−9.9	−18.3	−173 (4)	0	0
L_{da}	−24.9	−8.9	−33.8	−6.2	−10.0	−16.2	−171 (4)	3.1	6.2
L_{de}	−28.4	−0.5	−28.9	−6.5	−1.3	−7.8	−174 (4)	9.4	14.2
L_{ga}	−35.5	0.1	−35.4	−7.1	−1.2	−8.3	−174 (3)	7.7	5.7
R_A	−19.1	−0.4	−19.5	−5.1	−1.1	−6.2	−183 (3)	9.2	19.7
R_S	−17.6	−2.6	−20.2	−3.9	−2.6	−6.5	−182 (4)	4.6	9.3

[a] $E_{Inter} = E_{Elec} + E_{VDW}$ is the sum over all residue pairs between the two Val656-Ile680 sequences. ATVEG motif contribution : sum over all the residue pairs between the sequence motif of one helix and the Val656-Ile680 sequence of the second helix. Energy terms correspond to 1/2 ($E_{H1\rightarrow H2} + E_{H1\leftarrow H2}$) averaged over the last nanosecond of the simulation. Stability of the dimer: E_{Tot} :sum of intrahelical interactions E_{Intra} (including the nonbonded terms and the bonded terms (E_{Stress}: helix strains)) and interhelical interactions (E_{Inter}). E_{stress} and E_{Tot} are given relatively to the lowest value calculated for L_{dd}. Energy terms are averaged over 100 energy minimized configurations taken along the last ns trajectory. Values in parentheses are RMS. Energy units are expressed as kcal/mol.

dimer interface. These interactions exist in dimer L_{de} but only between Glu650 on one monomer and Arg652 on the other, permitting more flexibility. At the C-terminus Arg-Lys side chain interactions are observed only in dimer L_{ga} at a very low frequency.

It is noteworthy that interhelical H-bond was not detected between the two helices in dimer R_A neither between the N- and C-terminal residues nor between the two Glu side chains clearly oriented toward the lipids.

Interactions Results

The stability of the dimer in the DMPC bilayer results from the energetic balance between several contributions. These are helix stability (intrahelical interactions), giving information on strains induced by helix–helix proximity and surrounding lipids; residue–residue interactions (interhelical interactions), which measure helix–helix association; and helix–lipid interactions.

Helix–Helix Interactions: Dimer Stability. Data are given in Table I. Interaction energies are calculated on the Val656-Ile680 sequence to better identify the energetic contribution within the bilayer for each dimer. Calculations over the complete sequence would lead to erroneous results because of structural deviations at helix extremities.

Very favorable electrostatic interactions are observed in dimers L_{dd} and L_{da} owing to the presence of interhelical H-bonds contrary to the other dimers. Helix–helix packing is mainly mediated by van der Waals interactions, which are much lower in dimer L_{ga} where tight contacts are maintained between the interfacial residues all along the entire hydrophobic sequence (detailed below). All the left-handed models

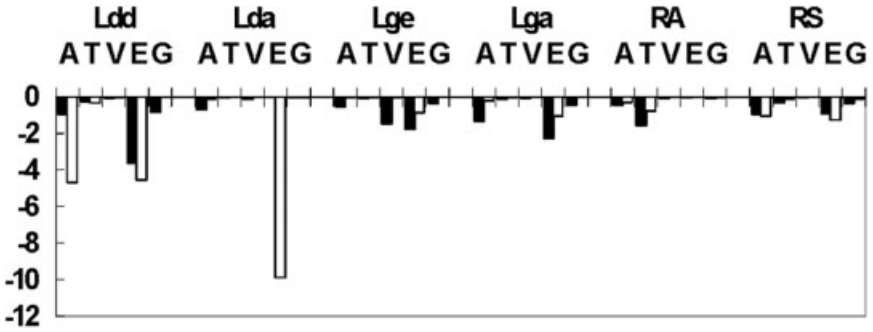

FIGURE 6 Interhelical interactions involving the five residue motif ATVEG in each $Neu^{E}{}_{TM}$ dimer model. Electrostatic energy ($E_{elec,}$ white bars) and van der Waals energy ($E_{VDW,}$ black bars) (in kcal/mol) are calculated as the sum of the energy terms over all the residue pairs involving one residue of the motif of one helix and all the residues of the Val656-Ile680 sequence of the second helix. Energy values correspond to 1/2 ($E_{H1\rightarrow H2} + E_{H1\leftarrow H2}$).

Table II Averaged Interaction with the DMPC and Water Environment per Monomer in the Neu^{E}_{TM} Dimers[a]

Dimer Model	Val656-Ile680 Sequence		Juxtamembrane Residues	
	DMPC	Water	DMPC	Water
L_{dd}	−102	−28	−244	−292
L_{da}	−98	−30	−173	−318
L_{de}	−89	−49	−124	−340
L_{ga}	−97	−47	−107	−343
R_A	−103	−36	−161	−329
R_S	−110	−33	−140	−282

[a]Interaction energies are given separately for the Val656-Ile680 sequence embedded in the bilayer core and the juxtamembrane residues including Glu650 to Pro655 at the N-terminus and Lys681to Arg684 at the C-terminus. The values (in kcal/mol) are the sum of electrostatic and van der Waals terms.

exhibit interhelical van der Waals interactions stronger than calculated for the right-handed models (about 10 to 17 kcal/mol in average).

The energetic importance of the ATVEG motif in helix–helix interactions is clearly evidenced. Motif–helix interactions are nearly half of helix–helix interactions in L_{dd} and L_{da} and only a third in R_A and R_S. Interestingly, motif–helix electrostatic interactions are generally stronger than between the two helices, indicating unfavorable interactions between few residues pairs. Weak positive energy values are observed at helix extremities and between residue pairs involving Gly665 (slightly positive value < 0.1 kcal/mol) in L_{dd}, L_{ga}, and R_A. van der Waals interactions involving the five residue motif are more favorable in the left-handed dimers, particularly for L_{dd}.

The energetic contribution of each residue motif in helix–helix packing is detailed in Figure 6, demonstrating the strong implication of Ala661 and Glu664 in helix–helix interaction in dimer L_{dd}. Only Glu664 plays a stabilizing role in dimer L_{da} but not in the other dimers.

A search of other stabilizing motifs was undertaken considering sequences including three, four, and five consecutive residues moving along the two helices. Two other motifs, $A_{653}SPVT_{657}$ and $T_{657}FIIA_{661}$, significantly contribute to helix–helix packing in R_S with motif–helix interactions of −6.4 and −9.5 kcal/mol, respectively, on average, equal or stronger than those calculated with the $A_{661}TVEG_{665}$ motif. Membrane protein sequence motifs containing polar Ser and Thr residues have an important role in stability.[28,73,74] In glycophorin A dimer a Thr residue in the GG4T4 motif accounts for additional interactions between the TM helices.[28,75]

Dimer L_{dd} is the most stable model resulting from the best compromise between intrahelical interactions and interhelical interactions and low energy strains. The right-handed dimer R_S exhibits the strongest intrahelical interactions but exhibits weak interhelical interactions.

DMPC and Water–Helix Interactions. Interactions with the environment are shown in Table II separately for the Val656-Ile680 sequence completely embedded in the bilayer core and the juxtamembrane residues located within the membrane interfaces.

Interaction energies between the residues embedded into the bilayer and the lipids are very favorable on the order of −100 kcal/mol on average per monomer, slightly stronger for the helices in dimer R_S. Energy terms associated with helix–water interactions are not negligible due to water penetration into the bilayer. Water molecules move from the upper layer (N-terminal side) toward residues Thr657 in all cases and Glu664 when the side chains extend close to the membrane interface. H-bonds between the carboxylic atoms and water can be formed 30 to 95% of the time except when the side chains point within the dimer interface (dimers L_{dd} and L_{da}). Water diffusion from the lower layer (C-terminal side) depends on the tilt of the helices and on helix structure and water molecules are observed close to Gly677 or more deeply close to the Val-rich sequence.

Interaction energies between the DMPC and the juxtamembrane residues are significantly stronger than estimated for the residues embedded in the bilayer core. For all the dimers interactions with water are very favorable as expected. The weakest helix–lipid interactions observed for L_{de} and L_{ga} are largely compensated by strong helix–water interactions mainly due to a complex hydrogen bond network formed by the Lys and Arg side chains extended within the bulk. In the particular case of dimer L_{dd}, interaction energies with the lipids and water are in the same order of magnitude on average and equally shared between the two monomers. This dimer interacts more favorably with the lipid environment by about 130 kcal/mol on average compared with the other dimers.

Dimer Interface

The dimer interface is completely characterized by calculating the Cα–Cα distance matrix between the residues on the two helices. The residues in close contact having the shortest Cα–Cα distances are given in Table III.

Table III Residue–Residue Distances between the Cα Atoms in the Neu^{E}_{TM} Dimers Given Along the Val656-Leu668 Sequence[a]

dimer	L_{dd}	L_{da}	L_{de}	L_{ga}	R_A	R_S	Neu^{V}_{TM}
H2	Residue on H1 d (Å)						
V656	F658 8.4		**S654 5.9**			A653 6.3	
T657	T657 6.2	T657 8.5		S654 7.2	S654 7.4	**A653 5.1**	**T657** 5.7
F658					**S654** 4.9	T657 7.2	F658 7.5
I659			T657 7.6		F658 7.0		
I660	A661 6.8	T657 7.3	T657 8.2	A661 6.5		T657 7.9	
A661	**A661 4.9**			A661 5.9	F658 7.5	A661 5.7	**A661 4.2**
T662					F658 5.9	A661 7.9	
V663		A661 8.2	A661 6.4		T662 8.5		
E664	G665 6.5	**A661 5.8**	E664 7.3	**G665 5.6**	G665 8.5		V664 7.3
G665	E664 7.1					G665 7.3	G665 6.5
V666			L668 7.6		T662 8.2		
L667	L668 7.7	E664 7.2	L668 5.4	L668 7.3	G665 7.2		
L668	L668 5.7	E664 7.5		L668 7.2		G665 8.4	L668 4.8
F669						L668 8.5	
L670			I671 7.0				
I671	L672 8.2			L668 7.9			
L672		E664 7.1					L672 5.7
V673							
V674			V675 7.9				
V675		L668 8.1		V675 7.0			
V676				V675 7.1			
G677							
I678				L679 7.9			
L679				L679 6.9			
I680							

[a]Residues on H2 are given in the first column. Residues on H1 are given only when the Cα-Cα distance is ≤ 8.5 Å. The closest residue pair is highlighted in bold in gray boxes. Contacting residues observed at the Neu^{V}_{TM} dimer interface (wild type) are indicated.[24] Note the similarity of the interface in model L_{dd}.

Contacting residue pairs are formed by identical residues in the symmetrical interface of dimer L_{dd}. A short distance is observed between the two Ala661 residues and other tight contacts are formed between the Thr657, Glu664, Gly665, Leu668, and Leu672 pairs. The same interfacial residues have been identified in the wild Neu_{TM} dimer model from Monte Carlo techniques.[24] Almost all of these residues are present at the helix–helix interface of the other left-handed dimers but in nonidentical residue pairs. Note that Gly665 is not at the inner interface in dimers L_{da} and L_{de}. L_{ga} is the only dimer for which tight contacts exist all along the helices until Leu679 near the membrane interface.

For the right-handed dimers the best residue contacts occur in the first part of the helices with the implication of residues Thr and Ser. The close approach of the two helices at the beginning of the sequence results in a large distance of separation between the C-terminal residues (> 12 Å).

Helix–helix packing of the left-handed structures is characterized by a contacting surface larger than in the right-handed structures (> 100 $Å^2$). However, for all the dimers, this surface is smaller in the DMPC bilayer than in vacuo (~ 20%), revealing helices less tightly packed.

Interestingly, the initial contacting surface involving the five-residue motif is conserved in L_{dd} but divided in half in R_S (~ 320 and ~ 220 $Å^2$, respectively, in the bilayer). This result reinforces the importance of this motif in helix–helix packing for the symmetrical left-handed dimer.

DISCUSSION

In this study we approach the question of the structure of the transmembrane domain of the oncogenic Neu receptor dimer. By using MD simulations we have

attempted to discriminate between correct and improper helix–helix packing by examining the structural and energetic properties of preformed left-handed and right-handed structures of the dimer in a membrane-like environment.

The limitations imposed by the slow dynamics of lipid bilayer precludes a rigorous analysis of the stability of the different structures of the dimers. A larger simulation (> 10 ns) conducted by us on the symmetrical left-handed dimer shows very similar geometric and energetic characteristics on average. Convergence of the left-handed structures would require a longer simulation time scale. A recent study showed that helix–helix packing interfaces in coiled coil dimers of polyleucine undergo minor changes in a 20-ns time scale of simulation,[76] thus transitions from asymmetrical to symmetrical arrangement of interhelical hydrogen bonding involving Glu cannot be reasonably expected during this time scale.

Besides the limitations of MD simulations associated with relatively short time scales, our results are in good agreement with general observations on membrane proteins and significant experimental data. We may then consider the dimer/DMPC systems realistic enough to describe reasonable properties of Neu^{E}_{TM} helix–helix packing.

Helix–helix crossing and helix tilt are on average close to those reported from polarized IR measurements.[23,77] Tilt of the dimers is accompanied by a slight expansion of the hydrophobic thickness of the lipid bilayer. These effects may reflect the response of the system to hydrophobic mismatch due to the greater length of the helices compared to the thickness of the DMPC bilayer.[78] Similar changes in the bilayer thickness observed in a pure DMPC simulation conducted with the same conditions[36] suggest that the bilayer expansion is mainly due to the simulation conditions with minor effects of the inserted helices.

An interesting finding is the π helix tendency of the Neu^{E}_{TM} helices in the dimers embedded in the DMPC bilayer, demonstrating that conformational flexibility is possible in the lipid environment. π bulge formation in $Neu/ErbB2_{TM}$ helices reported early from MD simulations[70] was recently confirmed in two separate NMR studies on the wild Neu^{V}_{TM} and Neu^{E}_{TM} monomers.[71,72] These results confirm anew that α–π–α motif formation in the Neu^{E}_{TM} helix is sequence dependent. Importantly, these properties may have a role in the activity, stability, and oligomerization process of Neu/ErbB2 receptors.[79]

Detailed analyses of the dimer/DMPC systems give insight into structural and energetic data not accessible from experiments. Simulations performed on the right-handed structure R_S reveal that the initial symmetry deduced from averaged Gly-Glu distances is not completely retained in the DMPC bilayer, resulting probably from helices not well packed. On the contrary, the symmetry of the left-handed dimer (L_{dd}) is correctly maintained. In all cases, helix–lipid interactions are in the same range of magnitude in the bilayer core, but the strongest interactions between the whole dimer and the lipid–water environment observed for the left-handed model L_{dd} demonstrate the most favorable anchor in the membrane. Helix orientation in dimer R_S impose inappropriate Glu side chain directions for strong interhelical H-bonds required for dimer stabilization whereas they were clearly evidenced in a DMPC : DMPS system.[77] The Thr657 hydroxyls are in the best position to hydrogen bond the facing Glu carboxyl groups. Interhelical side chain-backbone hydrogen bonds between Glu and Ala661 are strongly maintained in the left-handed dimer.

Most of the biological studies show the importance of the ATVEG motif in ErbB2/Neu receptor dimerization.[80–83] This motif is similar to the GxxxG motif that mediates the dimerization of glycophorin A.[28,29,84] This GG4 motif increases the total area of the helix–helix interface when helices cross in a right-handed sense.[30]

The present simulations show that contacting surfaces between the ATVEG motifs is 100 $Å^2$ greater in the left-handed structure L_{dd} than in the right-handed structure R_S. In addition, the strongest implication of the motif in helix–helix packing is obtained when helices cross symmetrically in a left-handed sense. Motif–helix interactions are about 50% of helix–helix interactions embedded in the bilayer core. Figure 7 shows how these residues are packed when helices are left-handed crossed in comparison with their packing in the right-handed structure.

Remarkably, this dimer model is almost indistinguishable to that obtained computationally using Monte Carlo simulations with the restriction of rigid ideal helices.[24] Both models bring out the close approach between the two Leu668 residues in total agreement with biological results.[18] These short interhelical distances at the C-terminal end, not present in the right-handed model, could provide additional experimental data, not yet observed from spectroscopic techniques, for defining the way the two helices wrap around one another.

None of the other dimer models fully explain the experimental data. The right-handed packing proposed from cysteine scanning studies[16] excludes the formation of interhelical Glu-Glu H-bonds. Glu side chain–side chain H-bond interactions in the asymmetrical dimers do not promote strong helix packing.

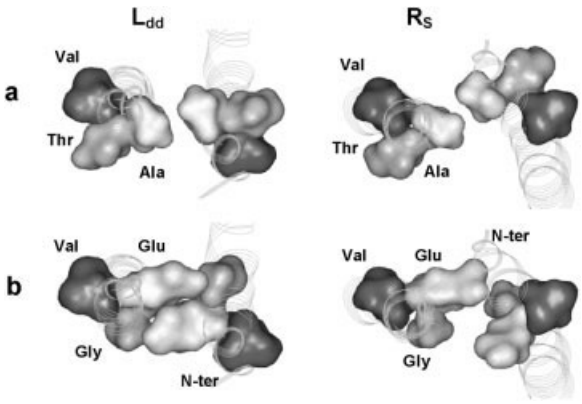

FIGURE 7 Helix–helix packing of the ATVEG residue-motif observed in the left-handed dimer L_{dd} and the right-handed dimer R_S at the end of the simulation in a DMPC bilayer. (a) ATV residue packing; (b) VEG residue packing. Residues are represented by their van der Waals surfaces. Helices are viewed form the N-terminal to the C-terminal [residues are labeled on H1 (left)]; the N-terminus is indicated on H2 (right). The difference in helix crossing angle is clearly shown. A particular good packing is seen in L_{dd}.

These dimer structures could describe intermediate states during the homodimerization process: side chain–side chain H-bonds might be a first step before the formation of Glu side chain-Ala backbone H-bonds and closer helix contacts. Such a hypothesis is consistent with a favored symmetrical arrangement of helices in support of energetic consideration that governs the interactions between identical subunits in a membrane.[85]

A symmetrical left-handed structure completely supports the nontransforming activity of the receptor mutants in which Glu replaces Val663 or Gly665.[86] Receptor inactivation was interpreted as a change in the dimer structure as a consequence of different but incorrect helix orientation in the receptor dimer. This same scenario could occur considering helices correctly oriented in the symmetrical left-handed structure. Modeling the replacement of Val or Gly by Glu leads to a large exposure of the side chains to the lipids (see Figure 7) and significant helix reorientation would be required for interhelical H-bond formation. On the contrary, the replacement of Gly by Glu in a right-handed packing similar to R_S shows that interhelical H-bond formation is possible without a change in helix orientation.

Moreover, it is quite logical to make a parallel between the nonactivation of the receptor mutant containing the glycophorin A motif,[82] which mediates right-handed interactions of the transmembrane segments, and the strong activation of the Neu^E receptor dimer with helices crossed in left-handed interactions. These two modes of helix association impose different directions to the helices and consequently to the catalytic domain via the juxtamembrane domain. As a result, the two tyrosine kinase domains in the receptor dimer would be oriented in an opposed fashion, one being favorable for tyrosine phosphorylation, the other not.

Molecular mechanisms by which constitutive activation arise through mutation are very probably similar for the Neu and ErbB2 receptors. Our present results with the Neu^E_{TM} dimers along with those obtained on the $ErbB2^E_{TM}$ dimer in a DMPC bilayer[36] argue for an active configuration of the receptor with the two helices in left-handed interactions. However, another interpretation was recently given for the $ErbB2^E_{TM}$ dimer, suggesting that, in the active state, a right-handed structure is driven by the N-terminal GxxxG motif.[26]

Although convergence of helix–helix packing is not reachable by MD simulation on a nanosecond time scale, the present study provides convincing results allowing the proposal that the active conformation of the transmembrane domain of the oncogenic Neu receptor could be a symmetrical left-handed structure with crossed Glu side chain/Ala backbone interhelical hydrogen bonds. This model provides a clear explanation of experimental data and sheds light on homooligomerization of the ErbB receptors. Such a structure may suggest further experiments and will help to develop targets to modulate receptor function for therapeutic purposes.

We are grateful to Pr S.O. Smith for providing the coordinates of the Neu_{TM} dimer, and J.P. Duneau and J. Sturgis for critical reading of the manuscript. This work was supported by the Centre National de la Recherche Scientifique (CNRS) and the Region Centre (France).

REFERENCES

1. Schlessinger, J. Cell 2000, 103, 211–225.
2. Hunter, T. Cell 2000, 100, 113–127.
3. Blume-Jensen, P.; Hunter, T. Nature 2001, 411, 355–365.
4. Burgess, A. W.; Cho, H. S.; Eigenbrot, C.; Ferguson, K. M.; Garrett, T. P.; Leahy, D. J.; Lemmon, M. A.; Sliwkowski, M. X.; Ward, C. W.; Yokoyama, S. Mol Cell 2003, 12, 541–552.
5. Garrett, T. P.; McKern, N. M.; Lou, M.; Elleman, T. C.; Adams, T. E.; Lovrecz, G. O.; Kofler, M.; Jorissen, R. N.; Nice, E. C.; Burgess, A. W.; Ward, C. W. Mol Cell 2003, 11, 495–505.
6. Ogiso, H.; Ishitani, R.; Nureki, O.; Fukai, S.; Yamanaka, M.; Kim, J. H.; Saito, K.; Sakamoto, A.; Inoue,

M.; Shirouzu, M.; Yokoyama, S. Cell 2002, 110, 775–787.
7. Fergusson, K. M.; Berger, M. B.; Mendrola, J. M.; Cho, H. S.; Leahy, D. J.; Lemmon, M. A. Mol Cell 2003, 11, 507–517.
8. Garrett, T. P.; McKern, N. M.; Lou, M.; Elleman, T. C.; Adams, T. E.; Lovrecz, G. O.; Zhu, H. J.; Walker, F.; Frenkel, M. J.; Hoyne, P. A.; Jorissen, R. N.; Nice, E. C.; Burgess, A. W.; Ward, C. W. Cell 2002, 110, 763–773.
9. Cho, H. S.; Mason, K.; Ramyar, K. X.; Stanley, A. M.; Gabelli, S. B.; Denney, D. W., Jr.; Leahy, D. J. Nature 2003, 421, 756–760.
10. Cho, H. S.; Leahy, D. J. Science 2002, 297, 1330–1333.
11. Franklin, M. C.; Carey, K. D.; Vajdos, F. F.; Leahy, D. J.; de Vos, A. M.; Sliwkowski, M. X. Cancer Cell 2004, 5, 317–328.
12. Stamos, J.; Sliwkowski, M. X.; Eigenbrot, C. J Biol Chem 2002, 277, 46265–46272.
13. Bargmann, C. I.; Hung, M. C.; Weinberg, R. A. Cell 1986, 45, 649–657.
14. Bargmann, C. I.; Weinberg, R. A. Proc Natl Acad Sci U S A 1988, 85, 5394–5398.
15. Weiner, D. B.; Liu, J.; Cohen, J. A.; Williams, W. V.; Greene, M. I. Nature 1989, 339, 230–231.
16. Burke, C. L.; Stern, D. F. Mol Cell Biol 1998, 18, 5371–5379.
17. Jiang, G.; Hunter, T. Curr Biol 1999, 9, R568–R571.
18. Bell, C. A.; Tynan, J. A.; Hart, K. C.; Meyer, A. N.; Robertson, S. C.; Donoghue, D. J. Mol Biol Cell 2000, 11, 3589–3599.
19. Binns, K. L.; Taylor, P. P.; Sicheri, F.; Pawson, T.; Holland, S. J. Mol Cell Biol 2000, 20, 4791–4805.
20. Wybenga-Groot, L. E.; Baskin, B.; Ong, S. H.; Tong, J.; Pawson, T.; Sicheri, F. Cell 2001, 106, 745–757.
21. Lofts, F. J.; Hurst, H. C.; Sternberg, M. J.; Gullick, W. J. Oncogene 1993, 8, 2813–2820.
22. Arteaga, C. L. Exp Cell Res 2003, 284, 122–130.
23. Smith, S. O.; Smith, C.; Shekar, S.; Peersen, O.; Ziliox, M.; Aimoto, S. Biochemistry 2002, 41, 9321–9332.
24. Kim, S. K.; Chamberlain, A. K.; Bowie, J. U. J Mol Biol 2003, 329, 832–840.
25. Cao, H.; Bangalore, L.; Dompe, C.; Bormann, B. J.; Stern, D. F. J Biol Chem 1992, 267, 20489–20492.
26. Fleishman, S. J.; Schlessinger, J.; Ben-Tal, N. Proc Natl Acad Sci U S A 2002, 99, 15937–15940.
27. Adamian, L.; Liang, J. J Mol Biol 2001, 311, 891–907.
28. Senes, A.; Gerstein, M.; Engelman, D. M. J Mol Biol 2000, 296, 921–936.
29. Lemmon, M. A.; Flanagan, J. M.; Hunt, J. F.; Adair, B. D.; Bormann, B. J.; Dempsey, C. E.; Engelman, D. M. J Biol Chem 1992, 267, 7683–7689.
30. MacKenzie, K. R.; Prestegard, J. H.; Engelman, D. M. Science 1997, 276, 131–133.
31. Sal-Man, N.; Gerber, D.; Shai, Y. Biochemistry 2004, 43, 2309–2313.
32. Lemmon, M. A.; Engelman, D. M. Q Rev Biophys 1994, 27, 157–218.
33. Caballero-Herrera, A.; Nilsson, L. Biophys J 2003, 85, 3646–3658.
34. Sajot, N.; Genest, M. Eur Biophys J 2000, 28, 648–662.
35. Sajot, N.; Genest, M. J Biomol Struct Dyn 2001, 19, 15–31.
36. Garnier, N.; Crouzy, S.; Genest, M. J Biomol Struct Dyn 2003, 33, 179–199.
37. Moriki, T.; Maruyama, H.; Maruyama, I. N. J Mol Biol 2001, 311, 1011–1026.
38. Gullingsrud, J.; Kosztin, D.; Schulten, K. Biophys J 2001, 80, 2074–2081.
39. Woolf, T. B.; Roux, B. Proc Natl Acad Sci U S A 1994, 91, 11631–11635.
40. Woolf, T. B.; Roux, B. Protein Struct Funct Genet 1996, 24, 92–114.
41. Bernèche, S.; Nina, M.; Roux, B. Biophys J 1998, 75, 1603–1618.
42. Roux, B.; Woolf, T. In Biological Membranes: A Molecular Perspective from Computation and Experiment; Merz, K. J.; Roux, B., Eds.; Birkhäuser: Boston, 1996; pp. 555–587.
43. Smith, S. O.; Aschheim, K.; Groesbeek, M. Q Rev Biophys 1996, 3, 252–258.
44. Nagle, J. F. Biophys J 1993, 64, 1476–1481.
45. Nagle, J. F.; Tristam-Nagle, S. Biochem Biophys Acta 2000, 1469, 159–195.
46. Brooks, B. R.; Bruccoleri, R. E.; Olafson, B. D.; States, D. J.; Swaminathan, S.; Karplus, M. J Comp Chem 1983, 4, 187–217.
47. MacKerell, J. A. D.; Bashford, D.; Bellot, M.; Dunbrack, R.L.; Evansek, J. D.; Field, M. J.; Fisher, S.; Gao, J.; Guo, H.; Ha, S.; Joseph McCarthy, D.; Kuchnir, L.; Kuczera, K.; Lau, F. T. K.; Mattos, C.; Michnick, S.; Ngo, T.; Nguyen, D. T.; Prodohm, B.; Reiher, W. E.; Roux, B.; Schlenkrich, B.; Smith, J.; Stote, R.; Straub, J.; Watanabe, M.; Wiorkiewicz-Kuczera, J.; Karplus, M. J Phys Chem B 1998, 102, 3585–3616.
48. MacKerell, J. A. D.; Bashford, D.; Bellot, M.; Dunbrack, R. L.; Evansek, J. D.; Field, M. J.; Fisher, S.; Gao, J.; Guo, H.; Ha, S.; Joseph McCarthy, D.; Kuchnir, L.; Kuczera, K.; Lau, F. T. K.; Mattos, C.; Michnick, S.; Ngo, T.; Nguyen, D. T.; Prodohm, B.; Reiher, W. E.; Roux, B.; Schlenkrich, B.; Smith, J.; Stote, R.; Straub, J.; Watanabe, M.; Wiorkiewicz-Kuczera, J.; Karplus, M. Biophys J 1992, 61, A143.
49. Schlenkrich, M.; Brickmann, J.; MacKerell, A. D. J.; Karplus, M. In Biological Membranes: A Molecular Perspective from Computation and Experiment; Merz, K. J.; Roux, B., Eds.; Birkhäuser: Boston, 1996; pp. 31–81.
50. Jorgensen, W. L.; Impey, R. W.; Chandrasekhar, J.; Madura, J. D.; Klein, M. L. J Chem Phys 1983, 79, 926–935.

51. Gennis, R. B. Biomembranes Molecular Structure and Function; Springer-Verlag: New York, 1989.
52. Belohorcova, K.; Qian, J.; Davis, J. H. Biophys J 2000, 79, 3201–3216.
53. Lague, P.; Zuckermann, M. J.; Roux, B. Biophys J 2001, 81, 276–284.
54. Petrache, H. I.; Grossfield, A.; MacKenzie, K. R.; Engelman, D. M.; Woolf, T. B. J Mol Biol 2000, 302, 727–746.
55. Ryckaert, J. P.; Ciccotti, G.; H. J. C., B. J Comput Phys 1977, 23, 327.
56. Bachar, M.; Becker, O. M. Biophys J 2000, 78, 1359–1375.
57. Bernèche, S.; Roux, B. Biophys J 2000, 78, 2900–2917.
58. Feller, S. E.; Pastor, R. W.; Rojnuckarin, A.; Bogusz, S.; Brooks, B. R. J Phys Chem 1996, 100, 17011–17020.
59. Chothia, C.; Levitt, M.; Richardson, D. J Mol Biol 1981, 145, 215–250.
60. O'Shea, E. K.; Klemm, J. D.; Kim, P. S.; Alber, T. Science 1991, 254, 539–544.
61. Killian, J. A.; von Heijne, G. Trends Biochem Sci 2000, 25, 429–434.
62. Arkin, I. T.; Brunger, A. T. Biochim Biophys Acta 1998, 1429, 113–128.
63. de Planque, M. R.; Killian, J. A. Mol Membr Biol 2003, 20, 271–284.
64. Lewis, B. A.; Engelman, D. M. J Mol Biol 1983, 166, 211–217.
65. Venable, R. M.; Zhang, Y.; Hardy, B. J.; Pastor, R. W. Science 1993, 262, 223–226.
66. Hoover, W. G. Phys Rev A, 1985, 31, 1695–1697.
67. Petrache, H. I.; Tristan-Nagle, S.; Nagle, J. F. Chem Phys Lipids 1998, 95, 83–94.
68. Nagle, J. F.; Zhang, R.; Tristram-Nagle, S.; Sun, W.; Petrache, H. I.; Suter, R. M. Biophys J 1996, 70, 1419–1431.
69. Bowie, J. U. J Mol Biol 1997, 272, 780–789.
70. Duneau, J. P.; Genest, D.; Genest, M. J Biomol Struct Dyn 1996, 13, 753–769.
71. Goetz, M.; Carlotti, C.; Bontems, F.; Dufourc, E. Biochemistry 2001, 40, 6534–6540.
72. Houliston, R. S.; Hodges, R. S.; Sharom, F. J.; Davis, J. H. FEBS Lett 2003, 535, 39–43.
73. Adamian, L.; Liang, J. Proteins 2002, 47, 209–218.
74. Dawson, J. P.; Weinger, J. S.; Engelman, D. M. J Mol Biol 2002, 316, 799–805.
75. Smith, S. O.; Song, D.; Shekar, S.; Groesbeek, M.; Ziliox, M.; Aimoto, S. Biochemistry 2001, 40, 6553–6558.
76. Ash, W. L.; Stockner, T.; MacCallum, J. L.; Tieleman, D. P. Biochemistry 2004, 43, 9050–9060.
77. Smith, S. O.; Smith, C. S.; Bormann, B. J. Nat Struct Biol 1996, 3, 252–258.
78. de Planque, M. R.; Goormaghtigh, E.; Greathouse, D. V.; Koeppe, R. E., 2nd; Kruijtzer, J. A.; Liskamp, R. M.; de Kruijff, B.; Killian, J. A. Biochemistry 2001, 40, 5000–5010.
79. Ubarretxena-Belandia, I.; Engelman, D. M. Curr Opin Struct Biol 2001, 11, 370–376.
80. Sternberg, M. J.; Gullick, W. J. Protein Eng 1990, 3, 245–248.
81. Cao, H.; Bangalore, L.; Bormann, B. J.; Stern, D. F. EMBO J 1992, 11, 923–932.
82. Burke, C. L.; Lemmon, M. A.; Coren, B. A.; Engelman, D. M.; Stern, D. F. Oncogene 1997, 14, 687–696.
83. Mendrola, J. M.; Berger, M. B.; King, M. C.; Lemmon, M. A. J Biol Chem 2002, 277, 4704–4712.
84. Russ, W. P.; Engelman, D. M. J Mol Biol 2000, 296, 911–919. 333
85. Arkin, I. T. Biochim Biophys Acta 2002, 1565, 347–363.
86. Bargmann, C. I.; Weinberg, R. A. EMBO J 1988, 7, 2043–2052.

Reviewing Editor: J. Andrew McCammon